A multiscale computational comparison of the bicuspid and tricuspid aortic valves in relation to calcific aortic stenosis

Eli J. Weinberg [a,b,c], Mohammad R. Kaazempur Mofrad [a,*]

[a] *Department of Bioengineering, University of California Berkeley, CA, USA*
[b] *Department of Mechanical Engineering, Massachusetts Institute of Technology, Cambridge, MA, USA*
[c] *Draper Laboratory, Cambridge, MA, USA*

ARTICLE INFO

ABSTRACT

Patients with bicuspid aortic valve (BAV) are more likely to develop a calcific aortic stenosis (CAS), as well as a number of other ailments, as compared to their cohorts with normal tricuspid aortic valves (TAV). It is currently unknown whether the increase in risk of CAS is caused by the geometric differences between the tricuspid and bicuspid valves or whether the increase in risk is caused by the same underlying factors that produce the geometric difference. CAS progression is understood to be a multiscale process, mediated at the cell level. In this study, we employ multiscale finite-element simulations of the valves. We isolate the effect of one geometric factor, the number of cusps, in order to explore its effect on multiscale valve mechanics, particularly in relation to CAS. The BAV and TAV are modeled by a set of simulations describing the cell, tissue, and organ length scales. These simulations are linked across the length scales to create a coherent multiscale model. At each scale, the models are three-dimensional, dynamic, and incorporate accurate nonlinear constitutive models of the valve leaflet tissue. We compare results between the TAV and BAV at each length scale. At the cell-scale, our region of interest is the location where calcification develops, near the aortic-facing surface of the leaflet. Our simulations show the observed differences between the tricuspid and bicuspid valves at the organ scale: the bicuspid valve shows greater flexure in the solid phase and stronger jet formation in the fluid phase relative to the tricuspid. At the cell-scale, however, we show that the region of interest is shielded against strain by the wrinkling of the fibrosa. Thus, the cellular deformations are not significantly different between the TAV and BAV in the calcification-prone region. This result supports the assertion that the difference in calcification observed in the BAV versus TAV may be due primarily to factors other than the simple geometric difference between the two valves.

© 2008 Elsevier Ltd. All rights reserved.

1. Introduction

The aortic valve opens to allow flow from the left ventricle to the aorta and closes to seal against backflow. This valve commonly has three cusps and three sinuses. In 1–2% of the population, however, the aortic valve has two cusps (Fedak et al., 2002), a condition known as a bicuspid aortic valve (BAV). Illustrations of tricuspid and bicuspid valve geometries are shown in Fig. 1. Serious complications develop in at least 33% of patients with BAV (Ward, 2000). The aortic valve is generally more susceptible to stenosis, regurgitation, and infection while the corresponding aorta is susceptible to medial degeneration, dilation and aneurysm, and dissection (Fedak et al., 2002). Of these, regurgitation is clearly a product of the malformed geometry of the BAV. The cause of the other complications is unclear at this time. It is conceivable that any of these diseases is more likely in patients with BAV due simply to the geometric difference between having two cusps and sinuses instead of three. For example, studies have examined whether creasing of the BAV leaflets gives rise to calcific aortic stenosis (CAS) (Robicsek et al., 2004a, b) and whether disrupted flow patterns in the BAV lead to aortic dilation (Bauer et al., 2006; Robicsek, 2003). Alternatively, the valves may have different mechanical properties that cause a difference in function that eventually leads the BAV to be more susceptible to disease than the tricuspid aortic valve (TAV). Another possibility is that the structural differences between the TAV and BAV are not relevant to whether the BAV is more likely to develop disease. Instead, BAV may be caused by a genetic defect, and this same defect independently gives rise to the other diseases. Fibrillin-1 deficiency has been notably implicated (Fedak et al., 2003).

* Corresponding author at: Molecular Cell Biomechanics Laboratory, Department of Bioengineering, University of California, 208A Stanley Hall #1762, Berkeley, UC94720-1762, USA. Tel.: +1 510 643 8165; fax: +1 510 642 5835.
 E-mail address: mofrad@berkeley.edu (M.R. Kaazempur Mofrad).
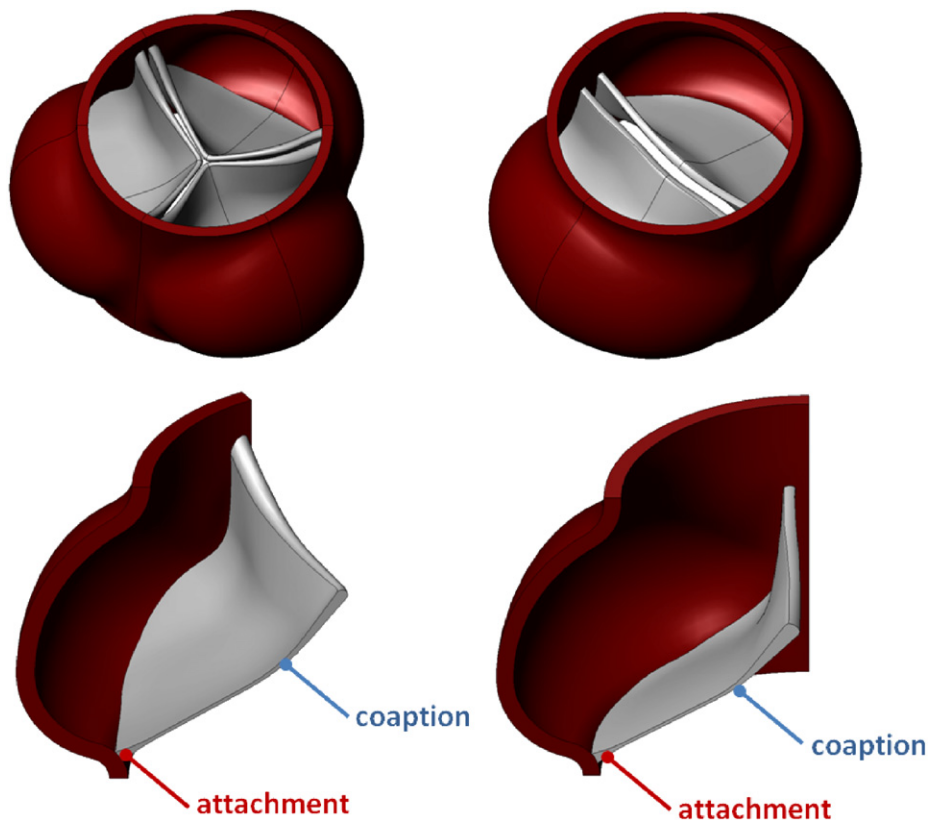
Fig. 1. Organ-scale valve geometries, tricuspid on left and bicuspid on right. Top: full geometry of valve. Bottom: cutaways showing tracking locations.

Much progress has been made in creating numerical simulations of heart valves over a range of length scales. Fluid-structure interaction models for organ-scale heart valve motion have been developed (De Hart et al., 2003; Einstein et al., 2005; Nicosia et al., 2003; Weinberg and Kaazempur Mofrad, 2007), allowing simultaneous prediction of the solid and fluid phases in the valve. At the tissue scale, many efforts have been made recently to formulate and implement appropriate experimentally-derived material constitutive models (Sacks and Yoganathan, 2007; Stella and Sacks, 2007; Weinberg and Kaazempur-Mofrad, 2005,2006). Cell-scale simulations have also been created with linkage to experimental data (Huang, 2004). Our group has recently developed a method for simulating mechanical behavior of the aortic valve across the range of length scales including cell, tissue, and organ, and verified the approach against experimental data for the normal tricuspid valve (Weinberg and Kaazempur Mofrad, 2007).

CAS progression is a multiscale process. Organ-scale stretches are translated to the tissue and cell scales, where dynamic deformations are imposed on the valvular interstitial cells (VICs). The VICs are thought to mediate the disease in response to these cellular deformations (Liu et al., 2007). Our multiscale simulation tools allow for examination of the multiscale disease mechanisms. In this study, we perform a multiscale analysis of the TAV and BAV in order to determine whether the increased incidence of CAS in the BAV may be linked to a mechanical difference between the two types of valve.

2. Methods

We have recently described a method for multiscale simulation of the tricuspid aortic valve (TAV) (Weinberg and Kaazempur Mofrad, 2007). Here, we briefly

outline the multiscale simulation methods we employ to compare the BAV and TAV. For further details including verification of the model versus experimental data, see Weinberg and Kaazempur Mofrad (2007). An overall schematic of this approach is shown in Fig. 2. Computed local deformations of the organ-scale model are projected as boundary conditions to the tissue-scale model. Similarly, local deformations of the tissue-scale model are mapped as boundary conditions to the cell-scale model.

First, we defined a system of reference configurations to describe the valve tissue deformations. Our system extends that of Stella and Sacks (2007). In Ω_0, the ventricularis and fibrosa are unattached and stress-free. The layers are connected to form the assembled tissue Ω_1. In Ω_2, the tissue is in position in a valve to which no pressure has been applied. When the valve is pressurized to its resting physiological state, the tissue is in Ω_3. We denote the time-varying state of the tissue in the functioning valve as Ω_t. Detailed illustration of these reference configurations can be found in Weinberg and Kaazempur Mofrad (2007).

The organ-scale simulation considers deformations from Ω_2 through Ω_t. The organ-level simulation was performed in LS-DYNA (LSTC, Livermore CA). This software was chosen because its operator-splitting method for fluid-structure interaction has been demonstrated to readily handle the motion of a solid through fluid typical of a functioning heart valve (Hallquist, 2006). LS-DYNA is an explicit solver, which means it may require excessive computation times in modeling relatively low-speed physical systems such as the aortic valves. We addressed this issue in our formulation of the constitutive model used to describe the cusp tissue mechanics.

To simulate the cusp mechanics, we have developed a constitutive model that describes the bulk material behavior and is particularly computationally efficient in explicit finite-element codes. Like many tissue constitutive models (Billiar and Sacks, 2000; Holzapfel et al., 2000; Sun and Sacks, 2005), our model treats the tissue as an isotropic solid with embedded aligned fibers. Instead of using a continuum model, though, we took a discrete approach. The solid mesh elements were modeled with an isotropic material. One-dimensional cable elements were then used to connect the nodes of the solid element. LS-DYNA allows assignment of arbitrary stress–strain curves to the cable elements, and fiber rotations follow nodal displacements. The inclusion of the fibers in the circumferential and radial directions helps capture the anisotropic nature of the tissue although the elements' material is defined as isotropic. This approach achieves enormous computational gains over a continuum approach; for further details see Weinberg and Kaazempur Mofrad (2007).
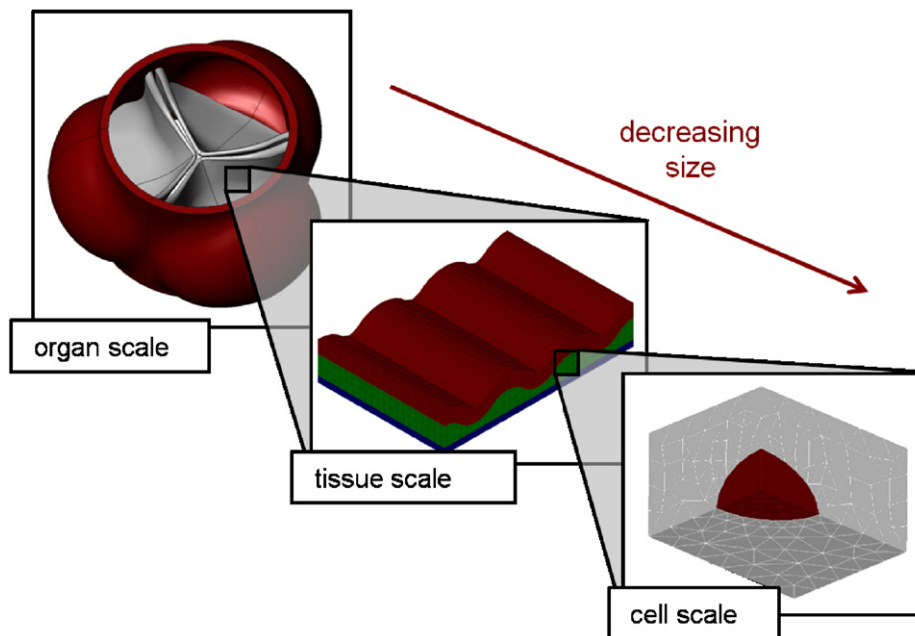
Fig. 2. Schematic of multiscale simulation approach. Deformations are mapped from largest scale to smallest.

The constitutive model was constructed referring to the tissue configuration Ω_2. The isotropic solid was modeled as a single-term Mooney–Rivlin with the value $C_1 = 2.0e4$ chosen to fit bending data for the leaflet (Huang, 2004; Sacks, 2001). The stress–strain curves in the radial and circumferential directions measured experimentally for configuration Ω_2 (Sacks and Yoganathan, 2007) were discretized and applied to the fiber elements. The aortic root was assumed to be isotropic and modeled with a single-term Mooney–Rivlin material. A value of $C_1 = 1.0e5$ was fit to experimental pressure-versus-dilation data for the root (Lansac et al., 2002). Further details on the development and validation of these models are outlined in Weinberg and Kaazempur Mofrad (2007).

Organ-scale geometry of the tricuspid and bicuspid valves were generated in SolidWorks (SolidWorks, Concord, MA). These solid geometries are shown in Fig. 1. This figure also illustrates the locations where local deformations were monitored for translation to the tissue-scale model. The tracking locations were chosen at two regions expected to show the highest degree of flexure: where the leaflet attaches to the wall (labeled "attachment"), and the hinge point where the coapted surface of the leaflet meets the free portion (labeled "coaption"). The overall geometry of the leaflets and sinuses (heights, lengths, angles, and diameters) for explanted valves have been measured and described in literature (Thubrikar, 1990). Finer geometric features, including the thickness distribution at different locations on the leaflet, have also been measured (Grande-Allen et al., 2001). Based on this collection of measurements, we created the valve geometry in SolidWorks in terms of two solid features: one loft for the sinus and one loft for the leaflet. In this way, the complete valve geometry is described by a small number of geometric variables and can readily be modified. Our CAD geometry represents the valve in the unstressed, unpressurized explanted state according to observations in our laboratory. For simplicity and to minimize computation time, the tricuspid valve is assumed to have $\frac{1}{6}$ symmetry and the bicuspid is assumed to have $\frac{1}{4}$ symmetry. The solid domain is embedded in a fluid domain having the same symmetry. Entry regions were added at both ends of the valve to allow the sinus to move radially, and fluid source domains were added at the orifices of the entry regions. Brick meshing is required in the fluid phase to utilize the operator-split method in LS-DYNA and our discrete-fiber constitutive model requires a brick mesh of the solid phase. Parametric 8-node brick meshes of both the solid and fluid domains were created in TrueGrid (XYZ Scientific Applications, Inc., Livermore CA). Cable elements representing circumferential and radial fiber families were overlaid on the solid mesh using HyperMesh (Altair Engineering, Troy MI), following observed fiber directions (Sacks et al., 1998).

Fixities and boundary conditions were applied to the mesh. Mirror conditions were applied to fluid and solid nodes on the two symmetry planes. The unattached ends of the entry regions were fixed while the nodes at the junction of the entry regions and the aortic root were constrained from moving axially. Outer faces of the fluid domain were not constrained. The same boundary conditions were applied to both the tricuspid and bicuspid models: experimentally-derived, time-varying pressure curves for the ventricle and aorta were applied to the appropriate fluid source domains (Thubrikar, 1990). An experimentally-derived radial displacement condition representing ventricular contraction was applied to the base
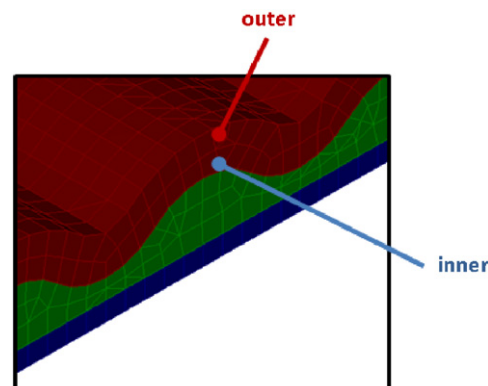

Fig. 3. Locations to track in tissue-scale simulation.

of the valve (Lansac et al., 2002). Pressures were slowly applied to bring the valve from its unpressurized state to its in-vivo resting position before the transient pressures were applied.

Post-processing was performed using HyperView (Altair Engineering, Troy MI). For both simulations, we recorded velocity profiles in the fluid phase and mechanical strains, displacements, and flexures in the solid phase throughout the solution.

Deformations from each organ-scale model were mapped as dynamic boundary conditions to tissue-scale models. Multilayered, undulated leaflet geometry was created in SolidWorks and meshed in ADINA (ADINA R&D, Watertown, MA). The geometry is illustrated in Fig. 3. An exponential, anisotropic constitutive model was developed and fit to experimental data (Stella and Sacks, 2007) for each layer. The region of interest, where calcification is observed to develop (Kuusisto et al., 2005; Otto, 2003), in the tissue-scale simulation is the layer closest to the aortic-facing leaflet surface, the fibrosa. To examine cellular deformations in this region, we recorded stretches in two locations of tissue-scale model, noted in Fig. 3. One location is on the outer edge of a curve in the fibrosa (labeled "outer"), and one location is on the opposing inner edge (labeled "inner").

Stretch data recorded in the tissue-scale models were mapped as boundary conditions to the cell-scale models. The cell-scale model is comprised of a cell in matrix. Geometry, shown in the cell-scale portion of Fig. 2, was created and meshed in ADINA. The cell was modeled by a single-term Mooney–Rivlin constitute relation (Huang, 2004) and the matrix was modeled using the constitutive model developed for the fibrosa in the tissue-scale model (Weinberg and Kaazempur Mofrad, 2007). We measure cellular deformations in terms of the cell aspect ratio (CAR), the ratio of

a cell's longest length dimension to its shortest (Huang et al., 2007; Weinberg and Kaazempur Mofrad, 2007). CAR was recorded versus time for the tricuspid and bicuspid valve, and the results compared to each other.

3. Results

Multiscale simulations linking cell-, tissue-, and organ-scale models were run to convergence with no instabilities. Computation time for the organ scale models was approximately 3 h for each cycle of opening and closing on a workstation with four Xeon 5160 3.00 GHz processors. Computation time for the cell and tissue models was a few minutes per cardiac cycle.

For the organ-scale model, deformed configurations of the TAV and BAV valves are illustrated at different times in Fig. 4 and flow fields at mid-systole are shown in Fig. 5. Overall dynamics of the tricuspid and bicuspid valves are similar. Since we defined the material properties, especially the extensibilities, to be the same in the leaflets and wall of the two valves, the leaflet strains and wall displacements had similar magnitudes and temporal trends. Two main differences were observed between the tricuspid and bicuspid valves. First, the bicuspid valve did not open fully, creating a jet in the fluid not seen in the tricuspid valve. Comparative velocity profiles at the aorta entrance are plotted in Fig. 6. Second, kinks formed in the bicuspid valve leaflet when open, whereas the tricuspid valve leaflets opened in smooth
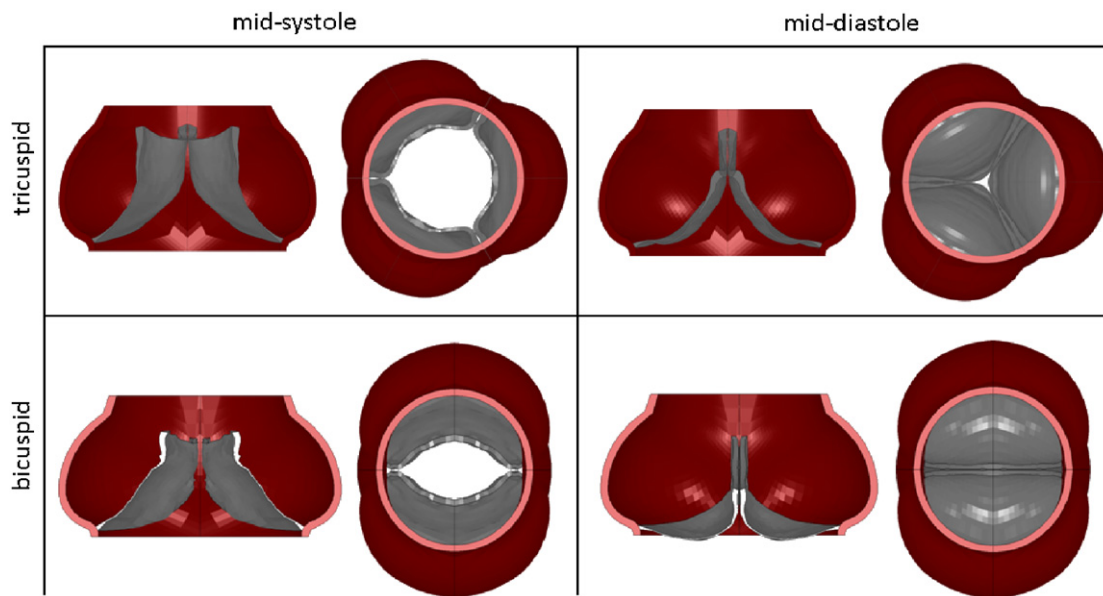

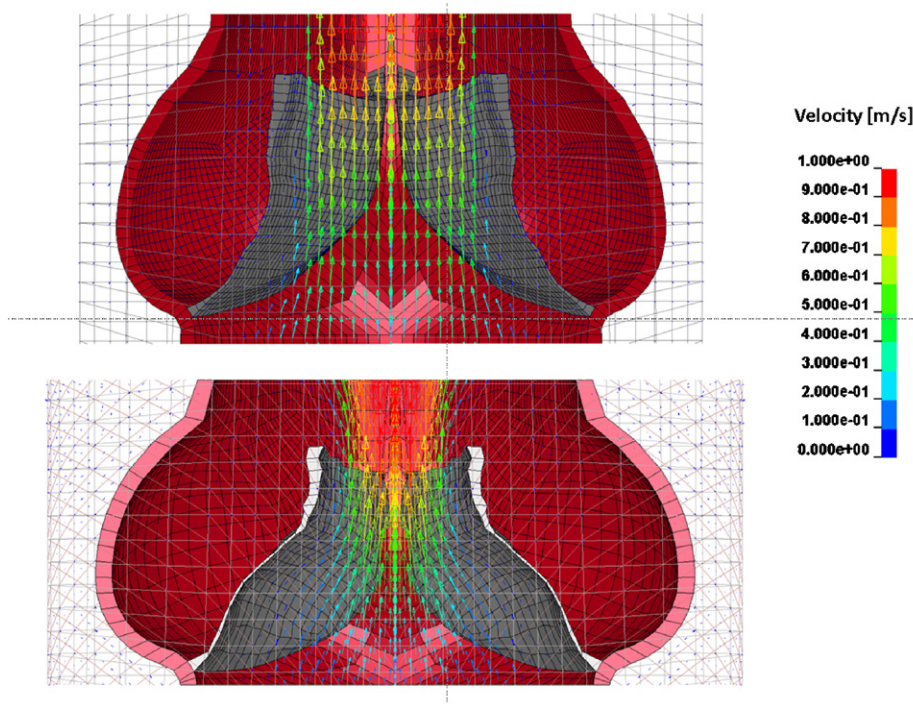Fig. 4. Predicted geometries of TAV and BAV at mid-systole and mid-diastole.

Fig. 5. Predicted flow fields in tricuspid (top) and bicuspid (bottom) valves at mid-systole.

curves. This effect is reflected in Fig. 7. In that figure, we have plotted the time-varying leaflet flexures in each valve measured at two points: where the leaflet attaches to the wall and where the coaption region begins. At each position, the bicuspid valve undergoes flexures of significantly greater magnitude than the tricuspid valve. Deformations were successfully mapped from the organ scale, through the tissue scale, to the cell-scale model.

Deformations at the tissue and cell-scale were recorded in the region of interest, near the aortic-facing surface of the leaflet, in the regions of highest organ-scale flexure. At the tissue scale, radial and circumferential stretches were recorded in the region of interest. Dynamic stretches for the TAV and BAV in the region of interest are plotted in Fig. 8. At the cell-scale, cellular aspect ratios were computed at the inner and outer locations of the region of interest, as illustrated in Fig. 3. Dynamic CARs for the TAV and BAV at these locations are plotted in Fig. 9. Both the tissue stretches and CARs in the region of interest are notably similar between the TAV and BAV relative to the large differences computed at the organ scale.

4. Discussion

We have created multiscale simulations of the TAV and BAV, where the only difference between the two simulations is the number of cusps. At the organ-scale, this geometric variation causes two major differences in function. Firstly, the leaflets of the bicuspid valve do not open as smoothly and undergo more flexure

relative to the normal tricuspid valve. Secondly, the bicuspid valve does not open as widely and the blood passing through the valve at systole forms a jet. Both differences in organ-scale behavior agree with experimental observations (Lewin and Otto, 2005; Robicsek et al., 2004a, b).

For both the TAV and BAV, deformations were mapped to tissue and cell length scales. Compared to the large differences
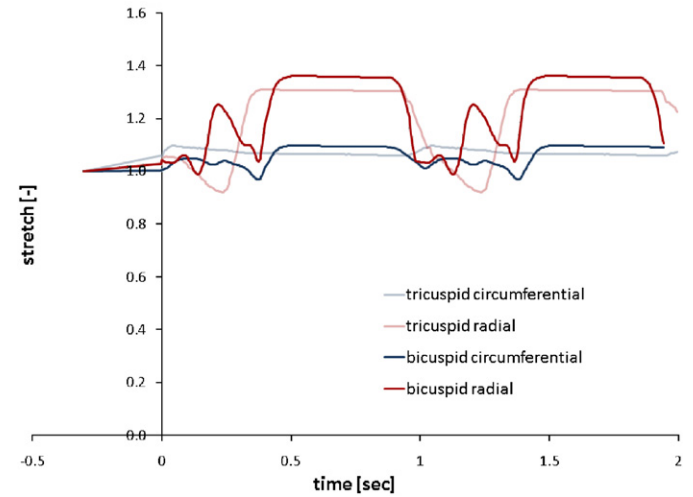

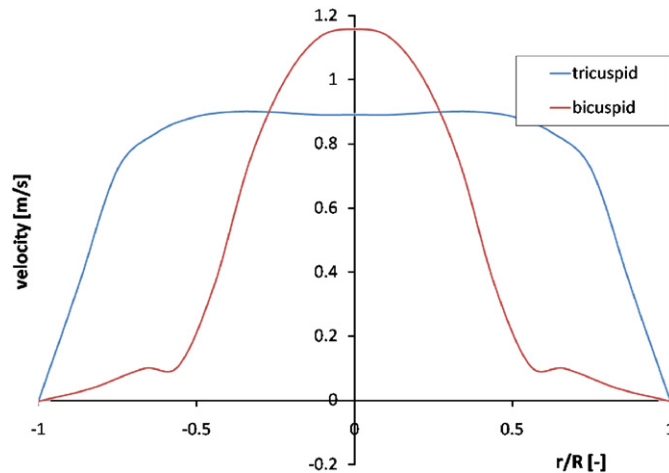**Fig. 8.** Dynamic stretches in region of interest for TAV and BAV.

Fig. 6. Fluid velocities versus radial position at entrance to aorta in tricuspid and bicuspid valves. *R* is radius of aortic orifice, 12 mm.
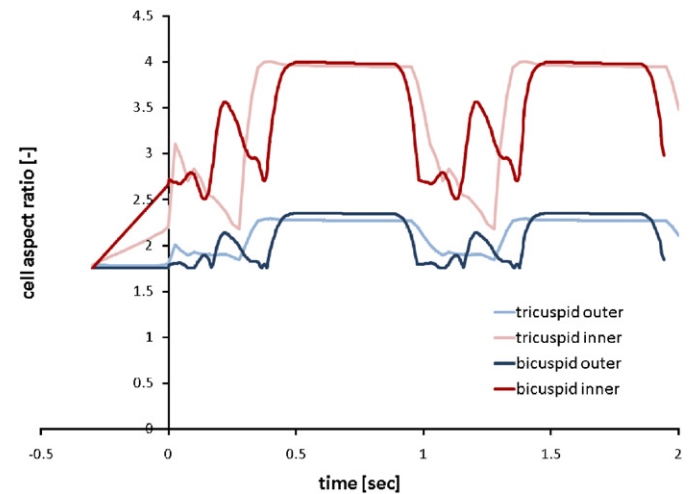

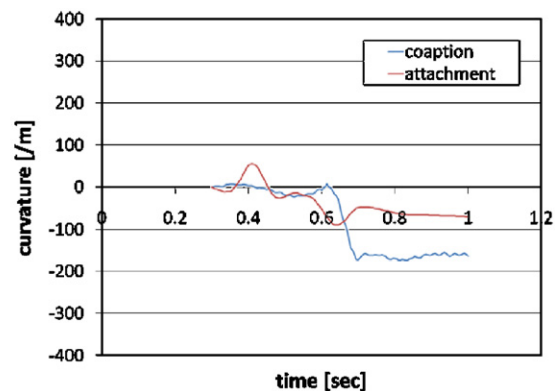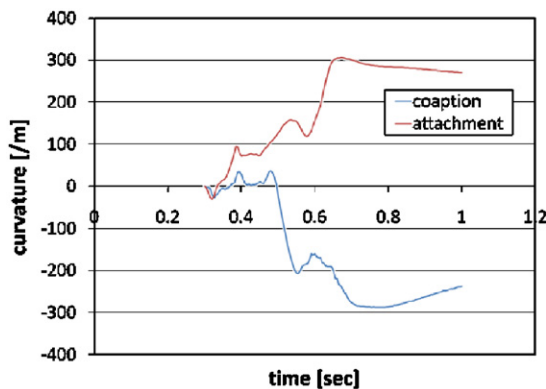**Fig. 9.** Dynamic cell aspect ratios in region of interest for TAV and BAV.

Fig. 7. Dynamic flexures in bicuspid (left) and tricuspid (right) valves.

computed at the organ scale, the differences between the BAV and TAV computed at the tissue and cell scales were small in the CAS-relevant region. We observed that the wrinkled structure of the fibrosa serves to shields the tissue, and the cells within, from strain. Thus, while greater deformations were seen in the bicuspid valve at the organ scale, we found that these differences did not translate down to the tissue or cell levels in the region of interest.

Since valvular interstitial cells (VICs) can only sense the cell-scale deformations, our model predicts that these cells experience similar mechanical stimuli in the TAV and BAV regardless of organ-scale differences. Thus, our results suggest that the observed difference in calcification between the TAV and BAV is not due to a difference in mechanical deformation. The difference in calcification may instead be due to a genetic difference which both determines the number of leaflets and the calcification risk. Evidence is mounting for a genetic cause of BAV (Cripe et al., 2004; Ellison et al., 2007), and that this genetic difference gives rise to a difference in the matrix constituents throughout the valve (Fedak et al., 2003). The fact that the BAV is more prone to a number of tissue diseases, including aortic dilation and aortic dissection, further suggests that the BAV is accompanied by dysfunctional tissue structure (Della Corte et al., 2007; Lewin and Otto, 2005; Otto, 2002). There remains the possibility that this difference in biochemical tissue structure between the BAV and TAV causes a difference in mechanical behavior, which then leads to deformations of the BAV that in turn lead to increased incidence of CAS. This effect could be investigated using our model if data on the mechanical properties of BAV were available. Currently they are not. Unless the BAV fibrosa structure is greatly different from that of the TAV, we would still expect to observe the strain-shielding effect on the cellular deformations in the region of interest that we found in the current study.

In this paper, we analyzed the mechanical differences between the tricuspid and bicuspid aortic valves over a range of length scales. We showed that cellular deformations in the region associated with CAS are not significantly different between the two valves. This result suggests that the difference in calcification risk between the two valves is not due to differences in deformation, and may instead be due to the genetic difference in matrix components.

Conflict of interest statement

This statement is to declare that we, Eli J. Weinberg, and Mohammad R. Kaazempur Mofrad, the authors of manuscript "*A Multiscale Computational Comparison of the Bicuspid and Tricuspid Aortic Valves in Relation to Calcific Aortic Stenosis*" do not possess any financial relationships that might bias our work. We hereby declare that no conflict of interest exists in our work.

Acknowledgements

References

Bauer, M., Siniawski, H., Pasic, M., Schaumann, B., Hetzer, R., 2006. Different hemodynamic stress of the ascending aorta wall in patients with bicuspid and tricuspid aortic valve. Journal of Cardiac Surgery 21 (3), 218–220.

Billiar, K., Sacks, M.S., 2000. Biaxial mechanical properties of the natural and glutaraldehyde treated aortic valve cusp—part II: a structural constitutive model. Journal of Biomechanical Engineering 122, 327–335.

Cripe, L., Andelfinger, G., Martin, L.J., Shooner, K., Benson, D.W., 2004. Bicuspid aortic valve is heritable. Journal of the American College of Cardiology 44 (1), 138–143.

De Hart, J., Peters, G.W.M., Schreurs, P.J.G., Baaijens, F.P.T., 2003. A three-dimensional computational analysis of fluid-structure interaction in the aortic valve. Journal of Biomechanics 36 (1), 103–112.

Della Corte, A., Bancone, C., Quarto, C., Dialetto, G., Covino, F.E., et al., 2007. Predictors of ascending aortic dilatation with bicuspid aortic valve: a wide spectrum of disease expression. European Journal of Cardio-Thoracic Surgery 31 (3), 397–404.

Einstein, D.R., Kunzelman, K.S., Reinhall, P.G., Nicosia, M.A., Cochran, R.P., 2005. Non-linear fluid-coupled computational model of the mitral valve. Journal of Heart Valve Disease 14 (3), 376–385.

Ellison, J.W., Yagubyan, M., Majumdar, R., Sarkar, G., Bolander, M.E., et al., 2007. Evidence of genetic locus heterogeneity for familial bicuspid aortic valve. Journal of Surgical Research 142 (1), 28–31.

Fedak, P.W.M., Verma, S., David, T.E., Leask, R.L., Weisel, R.D., et al., 2002. Clinical and pathophysiological implications of a bicuspid aortic valve. Circulation 106 (8), 900–904.

Fedak, P.W.M., de Sa, M.P., Verma, S., Nili, N., Kazemian, P., et al., 2003. Vascular matrix remodeling in patients with bicuspid aortic valve malformations: implications for aortic dilatation. Journal of Thoracic and Cardiovascular Surgery 126 (3), 797–806.

Grande-Allen, K., Cochran, R., Reinhall, P., Kunzelman, K., 2001. Finite-element analysis of aortic valve sparing: influence of graft shape and stiffness. IEEE Transactions on Biomedical Engineering 48 (6), 647–659.

Hallquist, J., 2006. LS-DYNA Theory Manual. Livermore.

Holzapfel, G.A., Gasser, T.C., Ogden, R.W., 2000. A new constitutive framework for arterial wall mechanics and a comparative study of material models. Journal of Elasticity 61 (1–3), 1–48.

Huang, H.-Y.S., 2004. Micromechanical Simulations of Heart Valve Tissues. University of Pittsburgh.

Huang, H.V.S., Liao, J., Sacks, M.S., 2007. *In-situ* deformation of the aortic valve interstitial cell nucleus under diastolic loading. Journal of Biomechanical Engineering-Transactions of the Asme 129 (6), 880–889.

Kuusisto, J., Rasanen, K., Sarkioja, T., Alarakkola, E., Kosma, V., 2005. Athero-sclerosis-like lesions of the aortic valve are common in adults of all ages: a necropsy study. Heart 91, 576–582.

Lansac, E., Lim, H.S., Shomura, Y., Lim, K.H., Rice, N.T., et al., 2002. A four-dimensional study of the aortic root dynamics. European Journal of Cardio-Thoracic Surgery 22 (4), 497–503.

Lewin, M.B., Otto, C.B., 2005. The bicuspid aortic valve: adverse outcomes from infancy to old age. Circulation 111, 832–834.

Liu, A.C., Joag, V.R., Gotlieb, A.I., 2007. The emerging role of valve interstitial cell phenotypes in regulating heart valve pathobiology. The American Journal of Pathology 171 (5), 1407–1418.

Nicosia, M.A., Cochran, R.P., Einstein, D.R., Rutland, C.J., Kunzelman, K.S., 2003. A coupled fluid-structure finite element modle of the aortic valve and root. The Journal of Heart Valve Disease 12, 781–789.

Otto, C.M., 2002. Calcification of bicuspid aortic valves. Heart 88, 321–322.

Otto, C.M., 2003. Valvular Heart Disease, second ed. Saunders, Philadelphia, PA.

Robicsek, F., 2003. Editorial: bicuspid versus tricuspid aortic valves. Journal of Heart Valve Disease 12 (1), 52–53.

Robicsek, F., Thubrikar, M.J., Cook, J.W., Fowler, B., 2004a. The congenitally bicuspid aortic valve: how does it function? Why does it fail? Annals of Thoracic Surgery 77, 177–185.

Robicsek, F., Thubrikar, M.J., Cook, J.W., Reames, M.K., Fowler, B.L., 2004b. Creases and folds: why does the bicuspid aortic valve fail so early? Journal of the American College of Cardiology 43 (5), 436A-A (Nw).

Sacks, M.S., 2001. The biomechanical effects of fatigue on the porcine bioprosthetic heart valves. Journal of Long Term Effects of Medical Implants 11 (3–4), 231–247.

Sacks, M.S., Yoganathan, A.P., 2007. Heart valve function: a biomechanical perspective. Philosophical Transactions of the Royal Society B 362, 1369–1391.

Sacks, M.S., Smith, D.B., Hiester, E.D., 1998. The aortic valve microstructure: effects of transvalvular pressure. Journal of Biomedical Materials Research 41 (1), 131–141.

Stella, J.A., Sacks, M.S., 2007. On the biaxial mechanical properties of the layers of the aortic valve leaflet. Journal of Biomechanical Engineering-Transactions of the Asme 129 (5), 757–766.

Sun, W., Sacks, M.S., 2005. Finite element implementation of a generalized fung-elastic constitutive model for planar soft tissues. Biomechanics and Modeling in Mechanobiology 4 (2–3), 190–199.

Thubrikar, M., 1990. The Aortic Valve. CRC Press, Boca Raton, FL.

Ward, C., 2000. Clinical significance of the bicuspid aortic valve. Heart 83 (1), 81–85.

Weinberg, E.J., Kaazempur-Mofrad, M.R., 2005. A large-strain finite element formulation for biological tissues with application to mitral valve leaflet tissue mechanics. Journal of Biomechanics 39 (8), 1557–1561.

Weinberg, E.J., Kaazempur-Mofrad, M.R., 2006. A finite shell element for heart mitral valve leaflet mechanics, with large deformations and 3D constitutive model. Journal of Biomechanics 40 (3), 705–711.

Weinberg, E.J., Kaazempur Mofrad, M.R., 2007. Transient, three-dimensional, multiscale simulations of the human aortic valve. Cardiovascular Engineering 7 (4), 140–155.